Supplement of Atmos. Chem. Phys., 24, 9805–9826, 2024
https://doi.org/10.5194/acp-24-9805-2024-supplement

Atmospheric Chemistry and Physics
Open Access
EGU

Supplement of

Measurement report: Vertical and temporal variability in the near-surface ozone production rate and sensitivity in an urban area in the Pearl River Delta region, China

Jun Zhou et al.

Correspondence to: Bin Yuan (byuan@jnu.edu.cn), Xiao-Bing Li (lixiaobing@jnu.edu.cn), and Min Shao (mshao@jnu.edu.cn)

S1. Supplemental figures to the main text

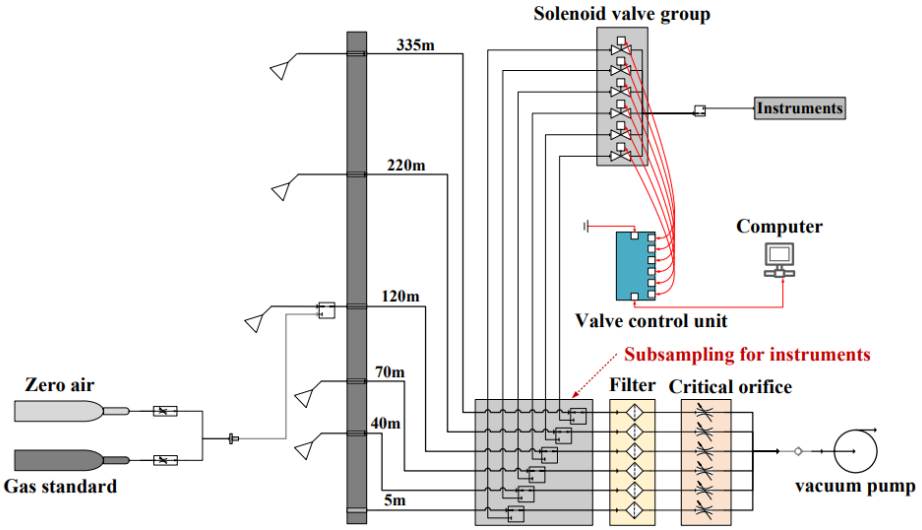

Figure S1. A simple schematic illustration of the vertical observation system on the SMT and locations of the six sampling inlets for measuring atmospheric gaseous species (Li et al., 2023).

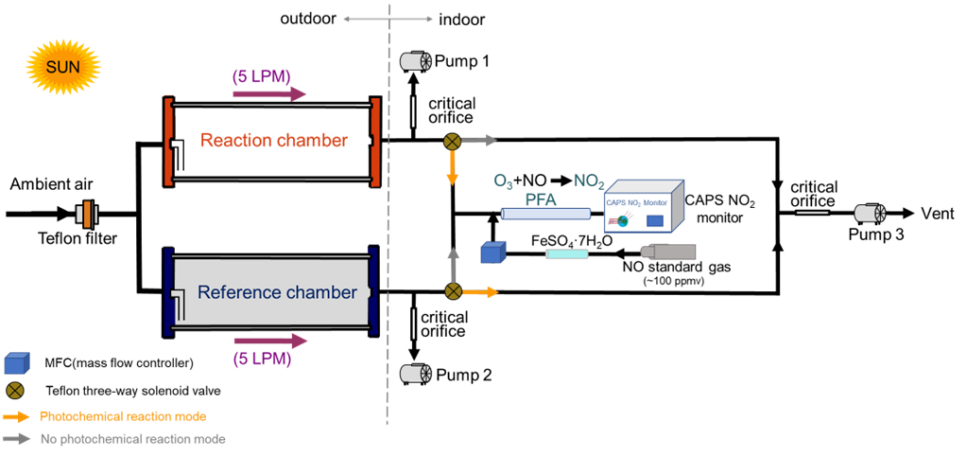

Figure S2. Schematic of the NPOPR detection system (Hao et al., 2023).

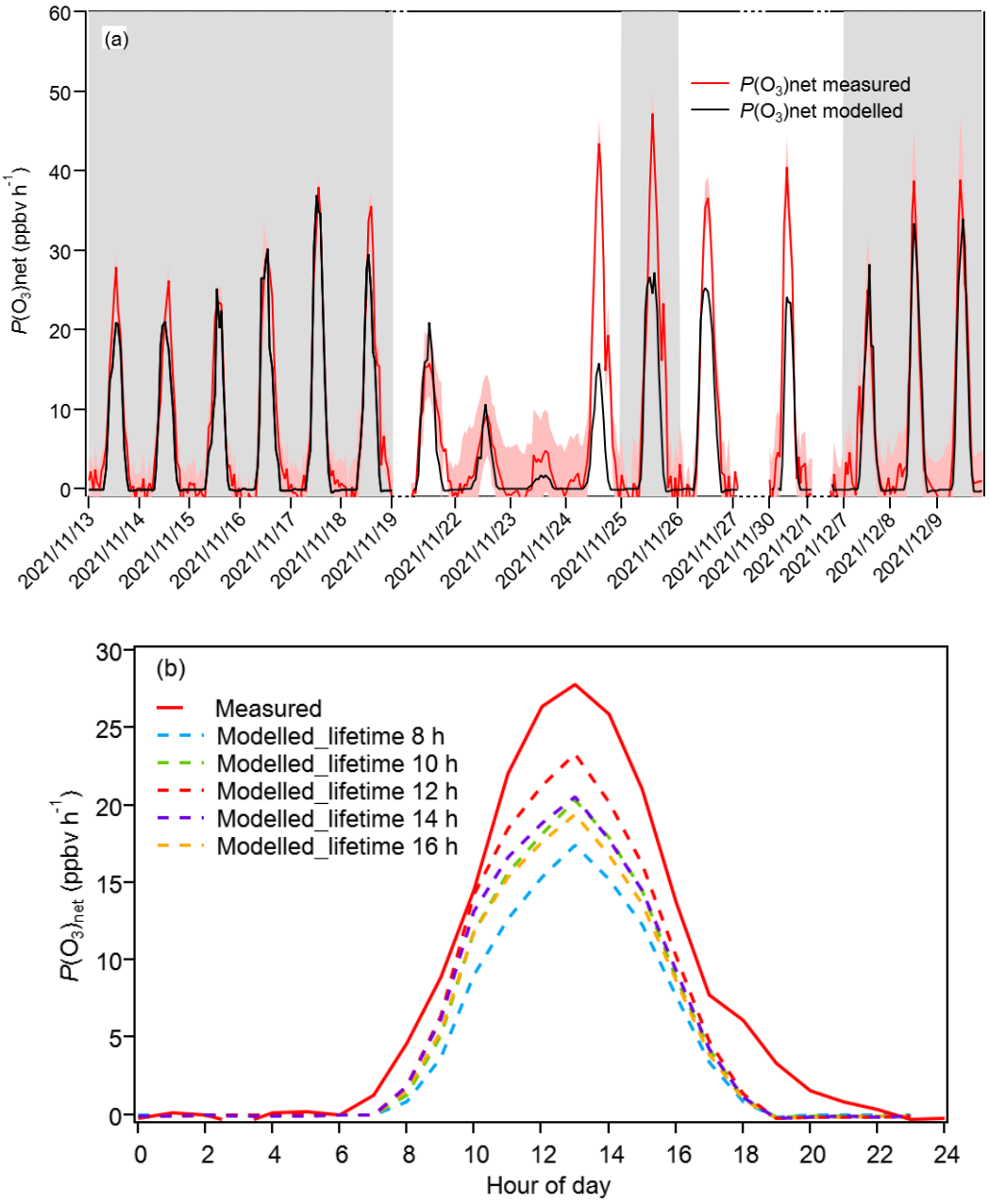

Figure S3. Measured and modelled $P(O_3)_{net}$ during the observation period from 13 November-9 December 2021.

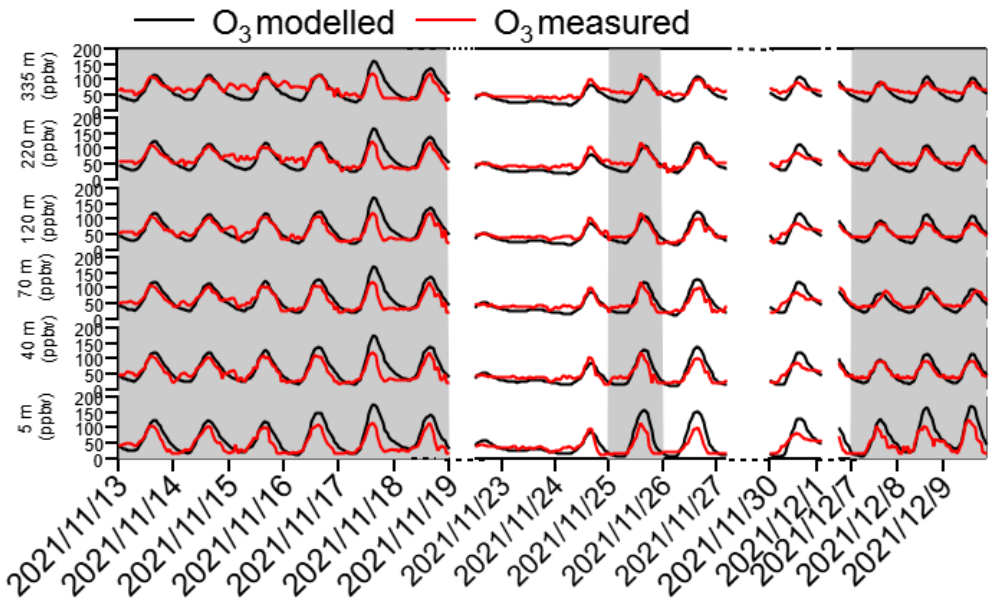

Figure S4. Measured and modelled O_3 concentrations at different heights during the observation period from 13 November-9 December 2021. The gray columns show the typical ozone episodes that occurred.

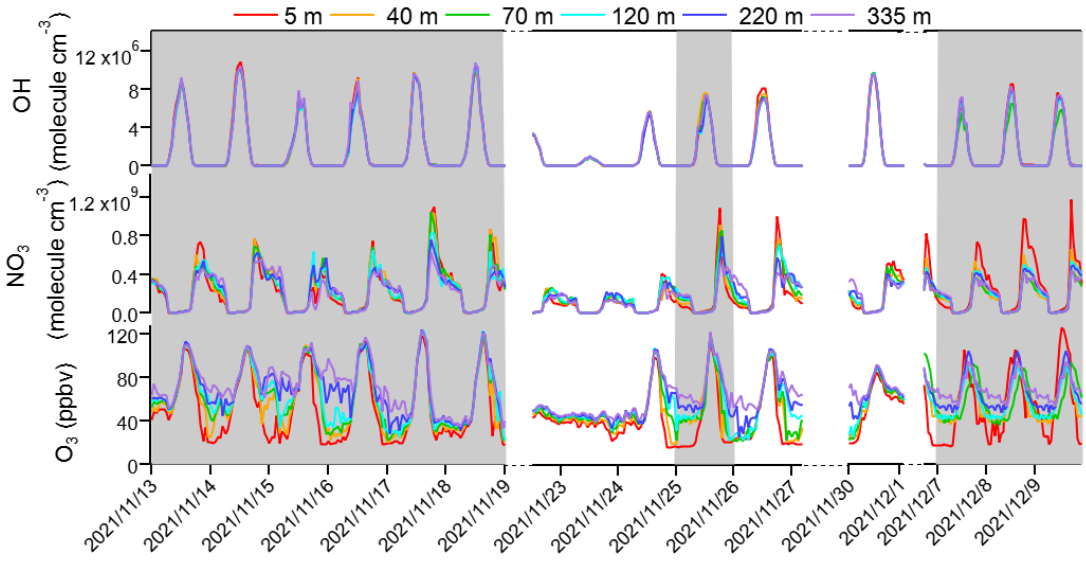

Figure S5. Time series of model-simulated OH and NO_3 concentrations in molecule cm^{-3}, and measured O_3 concentrations in ppbv at six different heights during 13 November-9 December 2021, at SZMGT, the gray columns show the typical ozone pollution episodes that occurred.

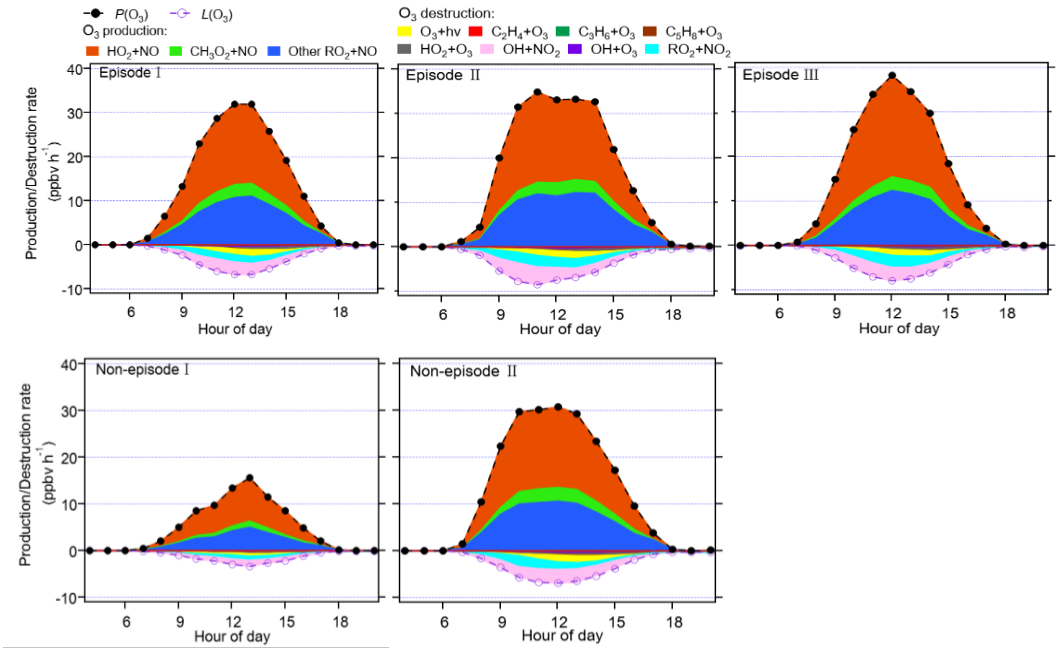

Figure S6. Average diurnal cycles of the model-simulated O_3 production and destruction rates at 5 m ground level during different episodes/non-episodes over the observation period.

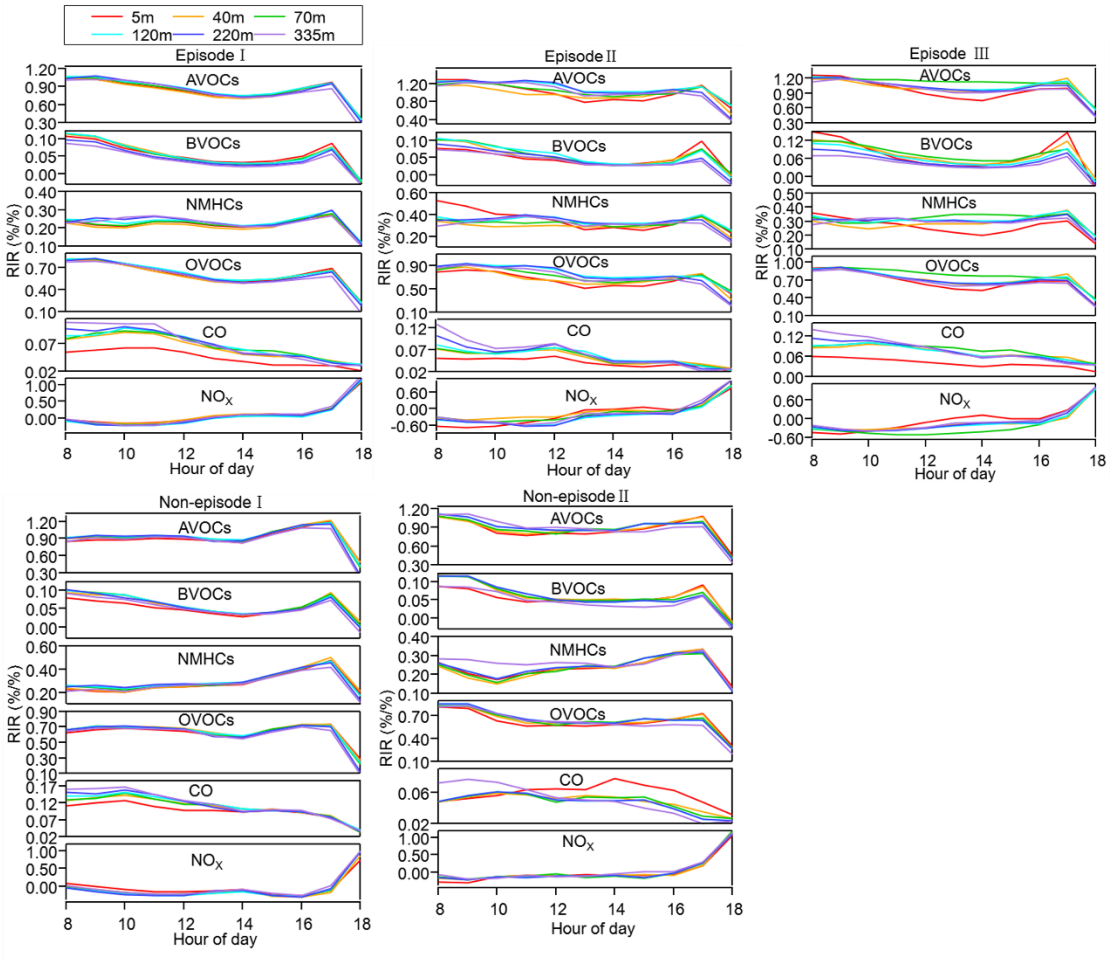

Figure S7. RIRs for O_3-precursor groups at different heights during local daytime (6:00-18:00).

S2. Supplemental tables to the main text

Table S1. Modelled O_3 production and destruction reactions and their reaction rates used in MCM in this study

Reactions	Rate coefficient / unit	Number
O_3 production pathways ($P(O_3)$)		
RO_2+ NO→RO + NO_2	$2.7\times10^{-12}\times\exp(360/T)$ / molecules $^{-1}$ cm^3 s^{-1}	(R1)
HO_2+ NO→OH + NO_2	$3.45\times10^{-12}\times\exp(270/T)$ / molecules $^{-1}$ cm^3 s^{-1}	(R2)
O_3 destruction pathways ($D(O_3)$)		
O_3 + hv → O^1D + O_2	Measured JO^1D / s^{-1}	(R3)
O_3 + C_2H_4 → HCHO + CH_2OOA	$9.1\times10^{-15}\times\exp(-2580/T)$ / molecules $^{-1}$ cm^3 s^{-1}	(R4)
O_3 + C_3H_6 → CH_2OOB + CH_3CHO	$2.75\times10^{-15}\times\exp(-1880/T)$ / molecules $^{-1}$ cm^3 s^{-1}	(R5)
O_3 + C_3H_6 → CH_3CHOOA + HCHO	$2.75\times10^{-15}\times\exp(-1880/T)$ / molecules $^{-1}$ cm^3 s^{-1}	(R6)
O_3 + C_5H_8 → CH_2OOE + MACR	$3.09\times10^{-15}\times\exp(-1995/T)$ / molecules $^{-1}$ cm^3 s^{-1}	(R7)
O_3 + C_5H_8 → CH_2OOE + MVK	$2.06\times10^{-15}\times\exp(-1995/T)$ / molecules $^{-1}$ cm^3 s^{-1}	(R8)
O_3 + C_5H_8 → HCHO + MACROOA	$3.09\times10^{-15}\times\exp(-1995/T)$ / molecules $^{-1}$ cm^3 s^{-1}	(R9)
O_3 + C_5H_8 → HCHO + MVKOOA	$2.06\times10^{-15}\times\exp(-1995/T)$ / molecules $^{-1}$ cm^3 s^{-1}	(R10)
O_3+ HO_2 → OH	$2.03\times10^{-16}\times(T/300)^{4.57}\times\exp(693/T)$ / molecules $^{-1}$ cm^3 s^{-1}	(R11)
RO_2+ NO_2 → peroxy nitrates	$(3.28\times10^{-28}\times7.24\times10^{18}\times P/T\times(T/300)^{-6.87}\times1.125\times10^{-11}\times(T/300)^{-1.105})\times10^{\wedge}(\log10(0.30)/(1+(\log10(2.916\times10^{-17}\times7.24\times10^{18}\times P/T\times(T/300)^{-5.765})/(0.75-1.27\times\log10(0.30)))^2))/(3.28\times10^{-28}\times7.24\times10^{18}\times P/T\times(T/300)^{-6.87}+1.125\times10^{-11}\times(T/300)^{-1.105})$ / molecules $^{-1}$ cm^3 s^{-1}	(R12)
NO_2+ OH → HNO_3	$(3.2\times10^{-30}\times7.24\times10^{18}\times P/T\times(T/300)^{-4.5})\times3\times10^{-11}\times10^{\wedge}(\log10(0.41)/(1+(\log10((3.2\times10^{-30}\times7.24\times10^{18}\times P/T\times(T/300)^{-4.5})/(3\times10^{-11}))/(0.75-1.27\times(\log10(0.41))))^2))/(3.2\times10^{-30}\times7.24\times10^{18}\times P/T\times(T/300)^{-4.5}+3\times10^{-11})$ / molecules $^{-1}$ cm^3 s^{-1}	(R13)
O_3+ OH → HO_2	$1.70\times10^{-12}\times\exp(-940/T)$ / molecules $^{-1}$ cm^3 s^{-1}	(R14)

Table S2. Measured VOCs concentrations during the observation periods at SZMGT (units: pptv).

Chemicals	Classification	Mean±SD (pptv)				
		Episode I	Episode II	Episode III	Non-episode I	Non-episode II
Aromatics		6738±5151	15147±8995	7107±5771	4748±3343	10530±10027
toluene	NMHC/ AVOC	3336±2496	7864±4298	3682±2648	2364±1697	5281±4919
m/*p*-xylene	NMHC/ AVOC	1444±1188	3097±2069	1390±1354	968±768	2223±2279

ethylbenzene	NMHC/ AVOC	613±504	1315±878	590±575	411±297	944±968
o-xylene	NMHC/ AVOC	593±489	1273±850	571±556	398±288	914±937
benzene	NMHC/ AVOC	445±227	819±349	527±316	382±182	654±399
styrene	NMHC/ AVOC	137±119	379±332	159±188	106±93	246±276
1,2,4-trimethylbenzene	NMHC/ AVOC	36±27	84±46	39±28	25±18	57±53
m-ethyltoluene	NMHC/ AVOC	35±26	82±45	38±28	25±18	55±51
p-ethyltoluene	NMHC/ AVOC	19±14	45±25	21±15	14±10	30±28
n-propylbenzene	NMHC/ AVOC	19±14	44±24	21±15	13±10	30±28
o-ethyltoluene	NMHC/ AVOC	18±14	43±24	20±15	13±9	29±27
isopropylbenzene	NMHC/ AVOC	12±9	28±15	13±10	9±6	19±18
1,2,3-trimethylbenzene	NMHC/ AVOC	11±8	26±14	12±9	8±6	17±16
*p*_diethylbenzene	NMHC/ AVOC	8±6	20±11	9±7	6±4	13±12
1,3,5-trimethylbenzene	NMHC/ AVOC	7±5	13±9	7±5	5±3	11±10
*m*_diethylbenzene	NMHC/ AVOC	4±3	10±6	5±3	3±2	7±6
OVOCs		39720±20318	66267±28451	48377±29973	26783±15486	47046±33037
methanol	OVOC/AVOC	8418±3917	15131±5681	10324±6640	6136±3448	10682±7116
formaldehyde	OVOC/AVOC	9449±4089	11853±3042	10562±4843	5303±3053	9165±4511
ethanol	OVOC/AVOC	7710±3756	14390±7288	10535±6910	6005±3201	10312±8417
acetone	OVOC/AVOC	4365±2953	7549±4676	5701±3897	2699±1586	4275±2829
hydroxyacetone	OVOC/AVOC	4047±2445	7007±2751	4543±3121	2766±1884	5448±4699
acetaldehyde	OVOC/AVOC	2532±1355	4367±1729	3007±1880	1697±956	3126±2244
methyl ethyl ketone	OVOC/AVOC	2310±1432	4723±2757	2715±2226	1653±984	3171±2722
acrolein	OVOC/AVOC	512±191	731±263	605±227	301±208	487±295
methyl vinyl ketone	OVOC/AVOC	179±70	207±80	185±98	89±73	170±78
methacrylaldehyde	OVOC/AVOC	124±49	144±55	128±68	62±51	118±54
m-cresol	OVOC/AVOC	50±40	97±50	46±41	43±25	55±37
phenol	OVOC/AVOC	24±20	66±79	26±22	28±18	36±35
Acetylene		1836±1259	3967±2168	1857±1336	1192±855	2664±2481
Acetylene	NMHC/ AVOC	1836±1259	3967±2168	1857±1336	1192±855	2664±2481
Alkanes		28108±21030	66256±36213	31017±22307	19916±14296	44495±41443
n-butane	NMHC/ AVOC	7972±5965	18793±10271	8797±6327	5649±4055	12620±11755
propane	NMHC/ AVOC	6417±4801	15127±8268	7081±5093	4547±3264	10159±9462
isobutane	NMHC/ AVOC	4513±3376	10637±5814	4980±3581	3198±2295	7144±6654
ethane	NMHC/ AVOC	3134±2345	7388±4038	3458±2487	2221±1594	4961±4621
isopentane	NMHC/ AVOC	1550±1160	3654±1997	1710±1230	1098±788	2454±2285

n-pentane	NMHC/ AVOC	1422±1064	3353±1832	1569±1128	1008±723	2251±2097
n-hexane	NMHC/ AVOC	574±429	1352±739	633±455	406±291	908±846
2-methylpentane	NMHC/ AVOC	428±321	1010±552	473±340	304±218	678±632
3-methylpentane	NMHC/ AVOC	383±286	902±493	422±304	271±195	606±564
3-methylhexane	NMHC/ AVOC	228±171	538±294	252±181	162±116	361±336
2-methylhexane	NMHC/ AVOC	177±132	417±228	195±140	125±90	280±261
cyclohexane	NMHC/ AVOC	176±	414±227	194±140	125±89	278±259
n-heptane	NMHC/ AVOC	161±121	380±208	178±120	114±82	255±238
methylcyclopentane	NMHC/ AVOC	113±85	267±146	125±90	80±58	180±167
2,3-dimethylbutane	NMHC/ AVOC	110±83	260±142	122±88	78±56	175±163
n-octane	NMHC/ AVOC	99±74	233±127	109±78	70±50	156±146
methylcyclohexane	NMHC/ AVOC	92±69	217±119	102±73	65±47	146±136
2,3-dimethylpentane	NMHC/ AVOC	86±64	203±111	95±68	78±56	136±127
2,2-dimethylbutane	NMHC/ AVOC	64±48	151±83	71±51	46±33	102±95
cyclopentane	NMHC/ AVOC	63±47	149±82	70±50	45±32	100±93
n-dodecane	NMHC/ AVOC	62±46	145±80	68±49	44±31	98±91
2,4-dimethylpentane	NMHC/ AVOC	49±37	116±64	54±39	35±25	78±73
n-decane	NMHC/ AVOC	44±33	104±57	49±35	31±22	70±65
n-nonane	NMHC/ AVOC	42±32	100±55	47±34	30±22	67±62
n-undecane	NMHC/ AVOC	37±28	88±48	41±30	26±19	59±55
3-methylheptane	NMHC/ AVOC	37±27	84±46	32±23	25±18	57±53
2-methylheptane	NMHC/ AVOC	29±21	68±37	39±28	20±15	45±42
2,2,4-trimethylpentane	NMHC/ AVOC	26±19	61±34	29±21	18±13	41±38
2,3,4-trimethylpentane	NMHC/ AVOC	19±14	44±24	21±15	13±10	30±28
Alkenes	NMHC/ AVOC	2202±1561	5043±2664	2492±1716	1530±1119	3422±3120
ethylene	NMHC/ AVOC	1494±1326	3187±1742	1492±1073	958±688	2141±1994
propylene	NMHC/ AVOC	412±365	878±480	411±296	264±190	590±549
1-butene	NMHC/ AVOC	163±145	348±190	163±117	105±75	234±218
1-pentene	NMHC/ AVOC	29±26	62±34	29±21	19±13	42±39
1-hexene	NMHC/ AVOC	15±13	31±47	15±11	9±7	21±20
trans-2-butene	NMHC/ AVOC	11±10	24±13	11±8	7±5	16±15
cis-2-butene	NMHC/ AVOC	11±10	24±14	11±8	7±5	16±15
trans-2-pentene	NMHC/ AVOC	5±4	10±6	5±3	3±2	4±4
cis-2-pentene	NMHC/ AVOC	3±3	6±3	3±2	2±1	7±6
isoprene	NMHC/ BVOC	277±185	471±165	351±176	156±132	351±260

Table S3. The median values of IOA, NMB, and NME between measured and modelled $P(O_3)_{net}$ (or O_3) for different episodes and non-episodes.

	Parameters	P1	P2	P3	C1	C2
IOA	$P(O_3)_{net}$	0.95	0.80	0.96	0.98	0.91
	O_3	0.86	0.78	0.84	0.73	0.71
NMB	$P(O_3)_{net}$	-0.16	-0.37	-0.10	-0.21	-0.25
	O_3	0.26	0.57	0.34	0.23	0.63
NME	$P(O_3)_{net}$	0.23	0.43	0.24	0.36	0.30
	O_3	0.32	0.59	0.40	0.42	0.65

Table S4. Top three VOCs species with the highest OFP (g cm^{-3}) values, for both NMHCs and OVOCs groups during various episodes and non-episodes.

Classification	Episode I	Episode II	Episode III	Non-episode I	Non-episode II
NMHCs	toluene 4.64E-11 *m/p*-xylene 3.37E-11 n-butane 2.07E-11	toluene 4.42E-11 *m/p*-xylene 2.96E-11 n-butane 1.98E-11	toluene 6.92E-11 *m/p*-xylene 4.44E-11 n-butane 3.09E-11	toluene 1.27E-10 *m/p*-xylene 8.34E-11 n-butane 5.69E-11	toluene 4.91E-11 *m/p*-xylene 3.31E-11 n-butane 2.19E-11
OVOCs	formaldehyde 1.12E-10 hydroxyacetone 3.33E-11 acetaldehyde 2.51E-11	formaldehyde 6.64E-11 hydroxyacetone 2.67E-11 acetaldehyde 1.96E-11	formaldehyde 1.5E-10 hydroxyacetone 4.82E-11 acetaldehyde 3.66E-11	formaldehyde 1.27E-10 hydroxyacetone 5.67E-11 acetaldehyde 4.34E-11	formaldehyde 8.44E-11 hydroxyacetone 3.03E-11 ethanol 2.27E-11

S3. The experiments concerning the light-enhanced loss of O_3

The light-enhanced loss of O_3 in the reaction and reference chambers at 5 L min^{-1} (the flow rate used during the observation campaign in this study) was investigated by carrying out the following outdoor experiment: the O_3 with a mixing ratio of approximately 130 ppbv generated by the O_3 generator (P/N 97-0067-02, Analytic Jena US, USA) was injected into both the reaction and reference chambers. We flowed zero air together with the generated O_3 into these chambers, which are located outdoors, to ensure there was no photochemical O_3 production. This setup allowed us to observe the real changes in photolysis frequencies of different species during daytime. The $J(O^1D)$, T, RH, P and O_3 mixing ratios at the inlet and outlet of the reaction and reference chambers were measured simultaneously. The T and RH were measured with a thermometer (Vaisala, HMP110, USA). The light-enhanced loss coefficient of O_3 (γ) was calculated using Eq. (2) described in the main text, and the relationship between $J(O^1D)$ and γ is shown in Fig. S8a. The obtained γ-$J(O^1D)$ equation listed in Fig. S8a was used to correct for the light-enhanced loss of O_3 in the reaction and reference chambers during the daytime to exclude the influence of light-enhanced loss. The change in the O_3 mixing ratio after correcting for the light-enhanced loss of O_3 ($d[O_3]$) showed no clear correlation with RH for both the reaction and reference chambers, as shown in Fig. S8b, indicating that the RH had no influence on the change in the O_3 mixing ratio during the observation period.

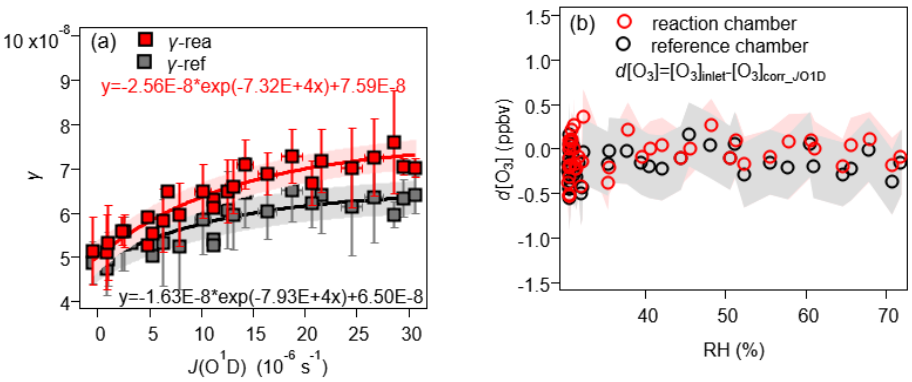

Figure S8: The relationship between (a) γ and $J(O^1D)$ and (b) RH and $d[O_3]$ in the reaction and reference chambers, calculated from the 68.3 % confidence interval of the fit lines between γ and $J(O^1D)$, the shaded areas represent the maximum range of fluctuation under this confidence level.

Furthermore, we quantified the light-enhanced loss of O_3 correction by comparing the $P(O_3)_{net}$ with and without the correction, the corresponding time series are shown in Fig. S9. Results show that such a correction can increase the measured $P(O_3)_{net}$ by 10% (25% percentile) to 24% (75% percentile), with the median value of 17%.

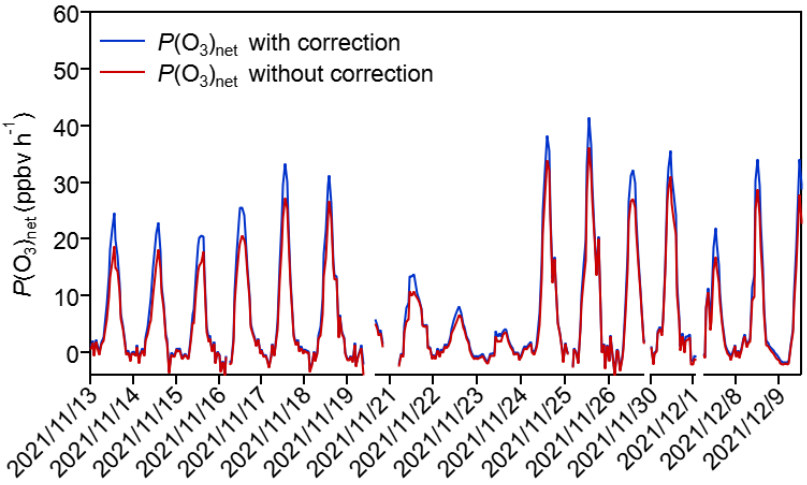

Figure S9: The time series of $P(O_3)_{net}$ with and without the light-enhanced loss of O_3 correction.

S4. Measurement error of $P(O_3)_{net}$ and the LOD of the NPOPR detection system

According to the $P(O_3)_{net}$ evaluation method listed in Eq. (1) in the main text, the measurement error of $P(O_3)_{net}$ depends on the estimation error of Ox in the reaction and reference chambers, which includes the measurement error of O_X of CAPS-NO_2 monitor and the error caused by γ, and can be calculated according to Eq. (S1) :

$$(O_X)_{error} = \sqrt{(O_{X_\gamma})_{error}^{2} + (O_{X_{CAPS}})_{error}^{2}} \quad (S1)$$

where $(O_X)_{error}$ represents the absolute error in the estimated O_X concentration in the reaction and reference chambers, which results from the quadratic propogation of the absolute errors $(O_{X_\gamma})_{error}$ and $(O_{X_{CAPS}})_{error}$. Here, $(O_{X_\gamma})_{error}$ denotes the error associated with the γ-corrected Ox of the chambers, while $(O_{X_{CAPS}})_{error}$ signifies the measurement error of the O_X measured by the CAPS-NO_2 monitor. The measurement error of the CAPS NO_2 monitor was obtained by fitting the NO_2 calibration results with a 68.3 % confidence level. The blue line in Fig. S10 represents the maximum range of fluctuation under this confidence level.

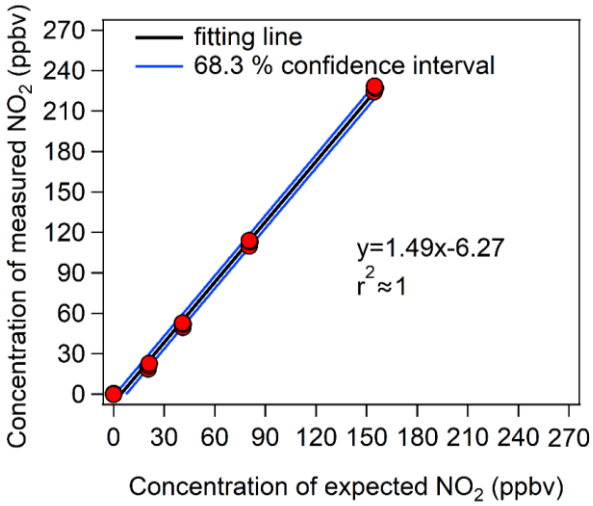

Figure S10: Calibration results of the CAPS NO_2 monitor at different NO_2 mixing ratios. The y-axis represents the NO_2 mixing ratios measured by the CAPS NO_2 monitor, and the x-axis represents the prepared NO_2 mixing ratios prepared from the diluted NO_2 standard gas.

$(O_{X_{CAPS}})_{error}$ was then calculated from the fluctuation range of the 68.3 % confidence interval of the calibration curve. The relationship between $(O_{X_{CAPS}})_{error}$ and the measured Ox value ($[Ox]_{measured}$) can be expressed as a power function curve, as shown in Eq. (S2):

$$(O_{X_{CAPS}})_{error} = 9.72 \times [O_X]_{measured}^{-1.0024} \quad \text{(S2)}$$

Dry pure air was sequentially introduced into the NPOPR detection system for ~ 2 h to adjust the system, followed by dry pure air or ambient air when the CAPS NO_2 monitor time resolution was 1 s and the integration period was 100 s (the measurement durations for the reaction and reference chambers were both 2 min). We acknowledge that this power function has been derived from calibration data of the O_X concentrations ranged from 20 ppbv to 160 ppbv. Utilizing this function outside this calibrated range, especially at very low O_X concentrations, may result in errors that are disproportionately large and may not accurately capture the true variability of the measurement errors. In this study, the O_X concentrations ranged from 28 to 145 ppbv, which falls into the calibration range. Consequently, this power function is deemed appropriate for estimating the $(O_{X_{CAPS}})_{error}$ throughout the whole measurement period.

The measured O_X errors may also be influenced by the light-enhanced loss of O_3

in the reaction and reference chambers under ambient conditions when the light intensity (especially $J(O^1D)$) and O_3 mixing ratios are high. Therefore, when injecting ambient air into the NPOPR system, the error of $P(O_3)_{net}$ with a residence time of τ can be calculated using Eq. (S3):

$$P(O_3)_{net\_error} = \frac{\sqrt{(O_{X_\gamma})_{rea\_error}^2 + ((9.72\times[(O_X]_{rea\_measured}^{-1.0024})_{rea\_std})^2 + (O_{X_\gamma})_{ref\_error}^2 + ((9.72\times[(O_X]_{ref\_measured}^{-1.0024})_{ref\_std})^2}}{\tau} \quad \text{(S3)}$$

where $(O_{X_\gamma})_{rea\_error}$ and $(O_{X_\gamma})_{ref\_error}$ represent the measurement error due to light-enhanced loss of O_3 in the reaction and reference chambers, respectively, and $(9.72\times[O_X]_{measured}^{-1.0024})_{rea\_std}$ and $(9.72\times[O_X]_{measured}^{-1.0024})_{ref\_std}$ represent the standard deviation of O_X in the reaction and reference chambers, respectively, caused by the CAPS NO_2 monitor with an integration time period of 100 s. Combined with the associated residence time $\langle\tau\rangle$ under different flow rates, i.e., $\langle\tau\rangle$ was 0.063 h at a flow rate of 5 L min^{-1}. In our previous research (Hao et al., 2023), we evaluated the residence time error and determined it to be approximately 0.0007, with an average residence time of 0.063 hours at a flow rate of 5 L min^{-1}. When we considered this error in the calculation of '$P(O_3)_{net}$_error', we observed a minimal reduction in the '$P(O_3)_{net}$_error' values, ranging from 0 to 2% [0.25-0.75 percentile]. This impact is considered negligible in relation to the overall '$P(O_3)_{net}$_error' as presented in Eq. 3. Consequently, we did not consider the uncertainty associated with the residence time in our calculations. We note that this collective measurement error of $P(O_3)_{net}$ is referred to as the measurement precision of the NPOPR detection system, which is different with the measurement accuracy of the NPOPR detection system described in Sect. 2.2.2.

The LOD of the NPOPR detection system was determined to be three times $P(O_3)_{net\_error}$. Since the measurement error of the CAPS NO_2 monitor decreases with increasing Ox mixing ratios (as shown in Eq. S2), higher LODs could be obtained when injecting dry pure air into the NPOPR detection system, which were approximately 0.07, 1.4, and 2.3 ppbv h^{-1} at air flow rates of 1.3, 3, and 5 L min^{-1}, respectively. Given that the background O_X mixing ratios (measured by the CAPS NO_2 monitor of the air in the reference chamber) changed when the ambient air was measured, the measured O_X

errors in the reaction and reference chambers changed with the Ox mixing ratios, and the LOD must also be a function of the intrinsic ambient and photochemically formed O_3 and NO_2 mixing ratios (i.e., the Ox mixing ratios measured by the CAPS NO_2 monitor).

References

Hao, Y., Zhou, J., Zhou, J. P., Wang, Y., Yang, S., Huangfu, Y., Li, X. B., Zhang, C., Liu, A., Wu, Y., Zhou, Y., Yang, S., Peng, Y., Qi, J., He, X., Song, X., Chen, Y., Yuan, B., and Shao, M.: Measuring and modeling investigation of the net photochemical ozone production rate via an improved dual-channel reaction chamber technique, Atmos. Chem. Phys., 23, 9891-9910, 10.5194/acp-23-9891-2023, 2023.

Li, X.-B., Zhang, C., Liu, A., Yuan, B., Yang, H., Liu, C., Wang, S., Huangfu, Y., Qi, J., Liu, Z., He, X., Song, X., Chen, Y., Peng, Y., Zhang, X., Zheng, E., Yang, L., Yang, Q., Qin, G., Zhou, J., and Shao, M.: Assessment of long tubing in measuring atmospheric trace gases: applications on tall towers, Environ. Sci.: Atmos., 3, 506-520, 10.1039/d2ea00110a, 2023.